Testing and analysing innovative design of UHPFRC anchor blocks for post-tensioning tendons

F. Toutlemonde, J.-C. Renaud & L. Lauvin
LCPC, Paris, France

M. Behloul
Lafarge, Paris, France

A. Simon
Eiffage TP, Neuilly-sur-Marne, France

S. Vildaer
VSL, Saint Quentin-en-Yvelines, France

ABSTRACT: Experimental validation of innovative design of anchor blocks for post-tensioning tendons was carried out. The tested specimens were made of UHPFRC, namely Ductal®-FM for 9 blocks and BSI® for 3 other blocks, and did not contain any passive reinforcement normally provided for confining concrete submitted to localized compression, and preventing bursting. They were dedicated to 4T15S, 7T15S and 12T15S pre-stressing units. Splitting in the middle of block sides, leading to sub-vertical cracks, appears as the dominant critical mechanism. Depending on lateral dimensions of UHPFRC around the reservation, and possible size effects concerning this zone submitted to intense tensile stresses, the maximum load has been obtained from 1,2 to 2,2 times the ultimate force of the tendons F_{prg}, with a typical scatter about ± 10 %. While refinements remain possible for optimizing the safety margin depending on project requirements, obtained results validate the innovative (reinforcement-free) design and typical dimensions of these UHPFRC anchor blocks.

1 INTRODUCTION

1.1 *Development of UHPFRC post-tensioned structures*

Ultra-high performance fiber-reinforced concrete (UHPFRC) represent an important breakthrough for civil engineering, limiting consumption of natural resources and leading to possibly optimal shapes for very durable structures. Important R & D efforts are currently undertaken in order to optimize structural application of these new materials, Bouteille & Resplendino (2005). Valuable structural application of UHPFRC ultra-high compressive strengths together with ductility requirements often leads to pre-stressed or post-tensioned solutions. Moreover, for structures made of pre-cast pre-stressed components, post-tensioning may represent an elegant assembly solution. Therefore, the question of safe design of end blocks for post-tensioning tendons is of high relevance.

In fact, confinement steel is normally provided in such anchor blocks for preventing the concrete bursting due to intense localized compressions, e.g. according to EN 1992-2: 2005. Specific experimental verifications have recently been carried out for extension of such provisions to very high performance concrete (C80 to C120), Boulay et al. (2004). Due to the high fiber content in UHPFRC, indirect tensile stresses due to the localized compressions may be taken by the fibers, so that conventional transverse confinement steel may not be necessary. Dispensing with conventional steel possibly allows a reduction of transverse dimensions of the end blocks, because the whole UHPFRC part is fiber-reinforced and there is no need for external cover. Optimal dimensions of UHPFRC end blocks can thus be considered as an important step towards rational and valuable development of these materials.

1.2 *Research significance*

Within the context of French R & D project MIKTI devoted to the development of new steel-concrete composite solutions, an experimental program dedicated to this question was carried out at LCPC. The reason of this comes from the related study of an optimized UHPFRC ribbed deck solution, made of segments assembled by post-tensioning, Toutlemonde et al. (2005).

This program tended to be more generic than previous validations of UHPFRC end blocks related to specific projects : Sherbrooke Footbridge, Ganz & Adeline (1997); Seonyu footbridge, Behloul et al. (2004); Millau toll gate, Hajar et al. (2004). Within the European context, the experiments should also give preliminary indications concerning application of the new standard agreement process, EOTA (2002), to these innovative solutions. Moreover, the results should be used for detailed analysis and possible further blocks optimization, given the companion exhaustive UHPFRC mechanical characterization carried out within the frame of the project.

2 EXPERIMENTAL PROGRAM

2.1 *Specimens*

The tested anchor blocks were made of UHPFRC, namely Ductal®-FM for 9 blocks and BSI® for 3 other blocks, and did not contain any classical passive reinforcement normally provided for confining concrete submitted to localized compression and preventing bursting of the anchor blocks. They were dedicated to 4T15S, 7T15S and 12T15S post-tensioning units. These units are considered as firstly interesting for possible application in rather thin structural shapes, based on design experience using such materials, Bouteille & Resplendino (2005). It had been chosen to reproduce the tests three times for each configuration, due to unknown scatter of expected results. The blocks had a square cross-section and an aspect ratio equal to 4, for ensuring absence of end effects on the zone which should be submitted to regularized compressive stresses after diffusion of localized compressions.

The innovative design allowed significantly reduced transverse dimensions of the blocks, given in Table 1. Blocks included a real-size sheath and the encased part of the pre-stressing kit in their central part. They were cast horizontally for purpose of being representative and including possible unfavourable orientation of the fibres. The real-size cylindrical plate where strands are clamped to was used for application of the localized compression on the block, with dimension given in Table 1. Due to proprietary units employed, dimensions of the steel end plate were fixed, as given in Table 2.

Table 1. Nominal dimensions of the specimens.

Ref	UHPFRC	kit type	unit	F_{prg}	side	heigth	load dia.
				kN	mm	mm	mm
1	Ductal®-FM	VSL	4T15	1116	160	640	110
2	Ductal®-FM	VSL	4T15	1116	160	640	110
3	Ductal®-FM	VSL	4T15	1116	160	640	110
4	Ductal®-FM	VSL	7T15	1953	185	740	135
5	Ductal®-FM	VSL	7T15	1953	185	740	135
6	Ductal®-FM	VSL	7T15	1953	185	740	135
7	Ductal®-FM	VSL	12T15	3348	255	1020	170
8	Ductal®-FM	VSL	12T15	3348	255	1020	170
9	Ductal®-FM	VSL	12T15	3348	255	1020	170
10	BSI®	Diwydag	7T15	1953	280	1120	130
11	BSI®	Diwydag	7T15	1953	280	1120	130
12	BSI®	Diwydag	7T15	1953	280	1120	130

Table 2. Dimensions of associated post-tensioning devices.

Ref	kit & unit	end plate Diameter	end plate Thickness	cone-shaped Length
		mm	mm	mm
1 to 3	VSL 4T15	120	10	180
4 to 6	VSL 7T15	145	10	180
7 to 9	VSL 12T15	200	25	360
10 to 12	Diwydag 7T15	170	18	82 + 170

2.2 *Testing procedure*

The testing program derived from the standard experimental procedure of ETAG 13 - European Technical Agreement Guide Nr 13 - EOTA (2002). Compressive axial loading was applied on the specimens, located vertically at the thrust center of a 5000 kN-capacity testing machine. During a first phase of the test, at least 10 loading cycles were applied from 0.12 to 0.8 times F_{prg}, until strains stabilization. Servo-control was based on load signal with an imposed rate corresponding to 0.5 MPa/s in the zone of regularized stresses. Then, loading was applied up to failure with a displacement-based control, at a rate of 0.5 mm/mn for the actuator. A safety limit of 10 mm-vertical displacement was authorized.

Centering of the samples was first ensured using lateral stops with respect to the bottom face. Control of lateral dimensions induce an uncertainty of about 1.5 % at this step. Axial centering was then verified, and if necessary favored, in case of uneven specimen thickness due to the casting phase (up to 1.5 % slope), with respect to the top side corresponding to the post-tensioning end.

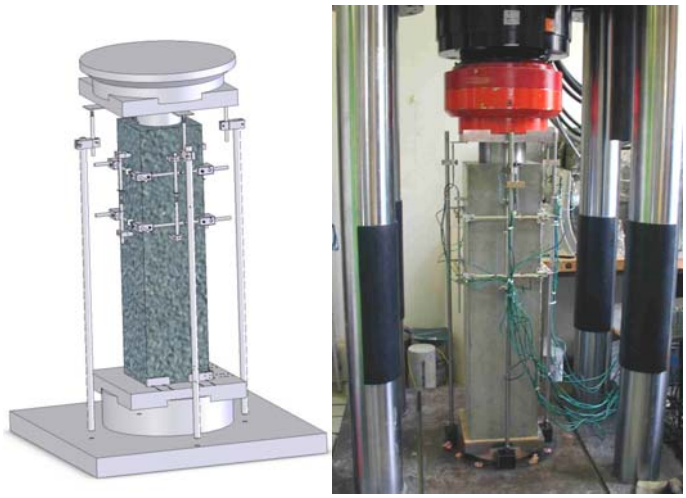

Figure 1. General testing and monitoring setup.

Besides load and actuator displacement monitoring, 16 measuring channels were recorded corresponding to identical numerical LVDT sensor equipment for all sides of the prisms. Transverse strains were measured from end to end of each side, at levels distant of 0.7 and 1.5 times the side length from the top of the block, using particular supporting devices already tested in Boulay et al. (2004). At a distance of 0.7 times the side length, tensile stresses are maximal in the reference computation of a homogenous elastic prism. Vertical strains were measured along the central axis of each side, between levels distant of 0.5 and 1.7 times the side length from the top of the block. Finally, the global vertical settlements were measured along the middle of each block side between the platens of the testing machine. A general view of the testing configuration is given (Fig. 1). One record was taken every 10 kN.

2.3 *Material characteristics*

Specimens 1 to 9 were made of Ductal®-FM, having a water to cement ratio equal to 0.21 and a volumetric fiber content equal to 2.15 %. Thermal treatment was applied at an age of 48 h, consisting in 48 hours exposure at 90°C and 95% RH. Average compressive strength measured on companion cylinders, 70 mm in diameter, was 190 MPa. Average specific gravity determined on the same specimens is 2.53 kg/m^3, Young's modulus 55 GPa and Poisson's ratio 0.17. Ductal®-FM characteristics in tension were identified on 7 cm x 7 cm x 28 cm prisms tested under bending. Average limit of linearity identified by 4-point bending of un-notched specimens corresponds to 16.3 MPa which is consistent with a design f_{tj} value equal to 9.6 MPa according to UHPFRC Recommendations, AFGC-SETRA (2002). Modulus of rupture identified by 3-point bending of 6 companion notched specimens reaches 35.4 MPa (average value) and 23.2 MPa (characteristic value).

Specimens 10 to 12 were made of BSI®. Average compressive 28 day-strength measured on companion cylinders stored in air, 110 mm in diameter, was 195 MPa (201 MPa when stored at 98 % RH). Young's modulus determined on similar cylinders ranges from 64 to 69 GPa. BSI® characteristics in tension were identified on prisms tested under bending. Average limit of linearity identified by 4-point bending of un-notched 7 cm x 7 cm x 28 cm specimens corresponds to 15.9 MPa which is consistent with a design f_{tj} value equal to 9.3 MPa according to UHPFRC Recommendations, AFGC-SETRA (2002). Modulus of rupture identified by 3-point bending of six 10 cm x 10 cm x 40 cm notched specimens reaches 35.6 MPa (average value) and 28.4 MPa (characteristic value).

Blocks were tested at an age of more than one year, so that UHPFRC strength and characteristics can be assumed as stabilized. From the identification here-above, it can be assumed that a direct tensile stress equal to about 9 MPa should correspond to cracking initiation, and that local hardening behavior with progressive parallel cracking, fibers re-anchoring and apparent ductility can be expected for a certain period at the structural level due to the significant margin between the maximum equivalent bending stress and the limit of linearity, and due to the significant enough stress gradients at the block scale.

3 GLOBAL RESULTS

3.1 *Blocks 1 to 3 for 4T15S units*

The global behavior of the blocks is represented in terms of applied load vs. average axial global displacement, including settlement at the ends, for blocks 1 to 3 (Fig. 2), after the first phase of cycles, which explains the non-zero origin of the curves. Maximum loads reached 2439, 2023 and 2085 kN respectively, which represents an average ratio of the ultimate load with respect to F_{prg} equal to 1.955. The minimum to maximum amplitude represents a variation of ± 9.5 %. In all cases after failure the load could be maintained to a value higher than F_{prg} provided displacement is controlled, not force (and even for block 1 some instability was noticed in a load / actuator displacement diagram).

Non-linearity before the peak is hardly significant on this global curve and shall be studied with information from more local survey. Namely, first (fine) cracks have been observed from 0.8 times F_{prg} (blocks 1 and 2) and 1.2 F_{prg} (block 3). As an example for block 1, evolution of this first crack (Fig. 3) in terms of opening and length took place significantly at 1.1 and 1.4 times F_{prg} respectively, and first cracks on another side were visible at 1.6 times F_{prg}. Transverse strains of block 1 at the most critical level (0.7 times the side length from the top side) are represented Fig. 4. Non-linearity is visible for loads

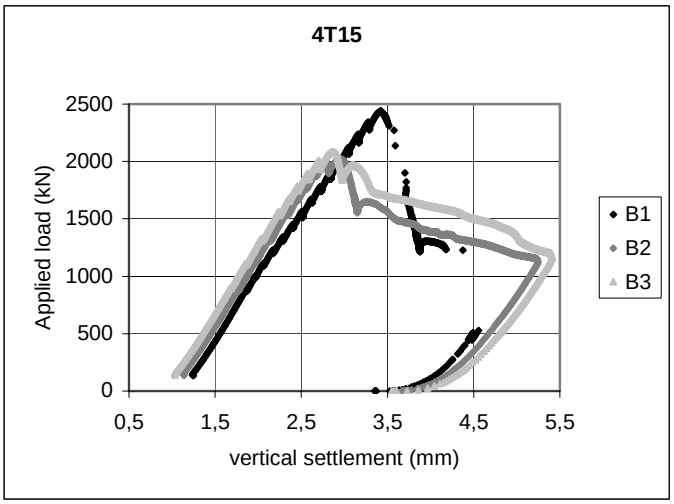

Figure 2. Load vs. axial global settlement, blocks 1 to 3.

Figure 3. Crack pattern evolution. Block 1 side D. (left) at first cracking - (right) after failure.

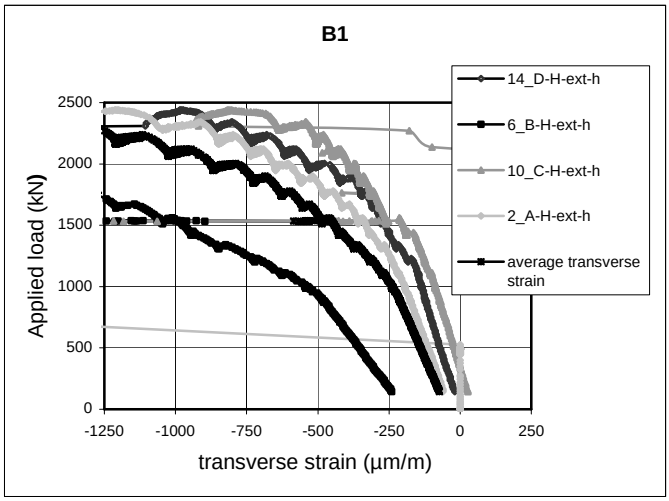

Figure 4. Block 1. Transverse strains at higher level (from top, 0.7 times the side length)

ranging from 0.85 to 1.3 times F_{prg}. Moreover, the side B with lowest apparent stiffness did not exhibit visible cracks before the final failure. Whatever the side, transverse displacements from side to side for a load variation equal to F_{prg} were kept below 40 µm, and strain "stabilization" in the sense of ETAG 013 had been obtained even on the less stiff side.

3.2 *Blocks 4 to 6 for 7T15S units*

The global behavior of the blocks 4 to 6 corresponding to 7T15S units is represented in terms of applied load vs. average axial global displacement, including settlement at the ends (Fig. 5), after the first phase of cycles, which explains the non-zero origin of the curves. Maximum loads reached 3058, 2735 and 2660 kN respectively, which represents an average ratio of the ultimate load with respect to F_{prg} equal to 1.443. The minimum to maximum amplitude represents a variation of ± 7.1 %. In all cases after failure the load could be maintained to a value close to F_{prg} provided displacement is controlled, not force (yet for blocks 4 and 6 some instability was noticed in a load / actuator displacement diagram).

Non-linearity becomes significant on this global curve somewhat below 2000 kN (close to F_{prg}). Considering information from more local survey, it turns out that first (fine) cracks have been observed from 0.8 times F_{prg} (blocks 5 and 6) and 1.0 F_{prg} (block 6). However even for block 4, non-linear evolution of transverse strains could be observed from about 1550 kN, i.e. 0.8 times F_{prg} (Fig. 6). But whatever the side of the block, transverse strains for a load variation equal to F_{prg} were kept below 250 µm/m, corresponding to transverse displacements from side to side lower than 50 µm, which is close to the conventional limit of one visible crack. Moreover, the first cracks were not observed on the side where non-linearity or non-stabilization of transverse strains first appeared.

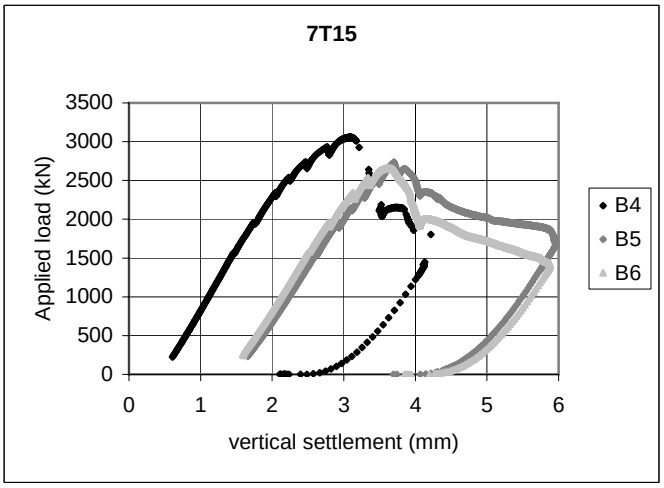

Figure 5. Load vs. axial global settlement, blocks 4 to 6.

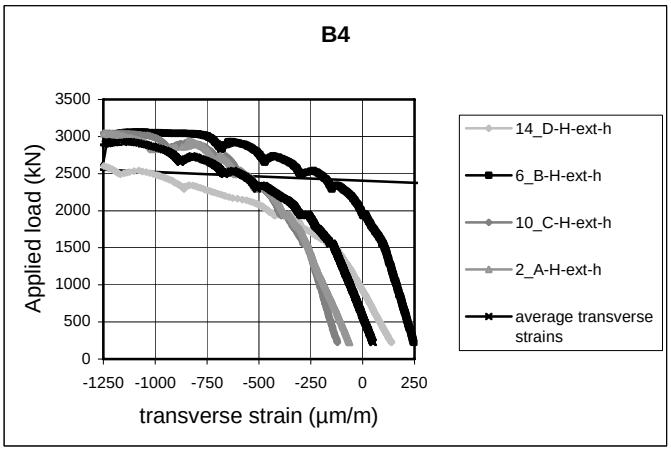

Figure 6. Block 4. Transverse strains at higher level (from top, 0.7 times the side length)

3.3 *Blocks 7 to 9 for 12T15S units*

The global behavior of the blocks 7 to 9 is represented in terms of applied load vs. average axial global displacement, including settlement at the ends, for these blocks corresponding to 12 T15S units (Fig. 7), after the first phase of cycles, which explains the non-zero origin of the curves. Maximum loads reached 4587, 4312 and 4182 kN respectively, which represents an average ratio of the ultimate load with respect to F_{prg} equal to 1.302. The minimum to maximum amplitude represents a variation of ± 4.7 %. In all cases reaching of the peak load was closely followed by important transverse strains at the top of the block, and concomitant buckling of the conical part of the pre-stressing duct was observed (Fig. 8). Onset of this instability (difficult control of the testing machine actuator, even displacement-controlled, due to transverse possible bursting – Fig. 9 - corresponds to a significantly less efficient confinement effect of the UHPFRC block (relative side dimensions of the block are lower than for Blocks 1 to 6, in correspondence with expected F_{prg}).

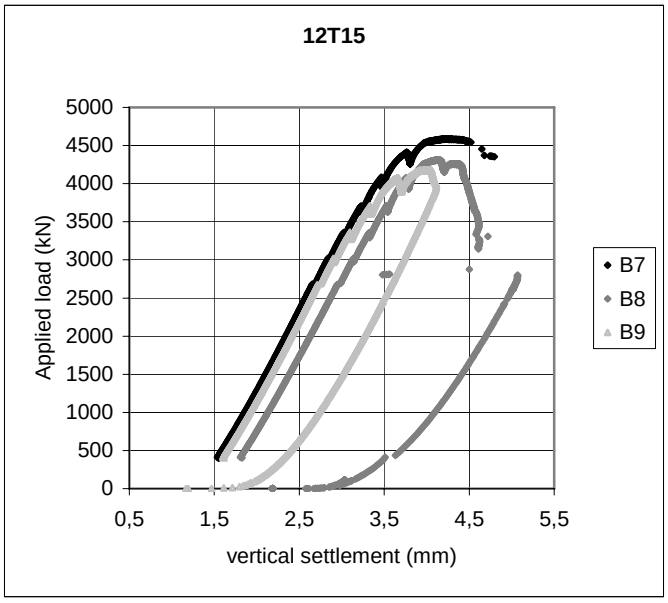

Figure 7. Load vs. axial global settlement, blocks 7 to 9.

Figure 8. Local buckling of the duct at failure, block 7.

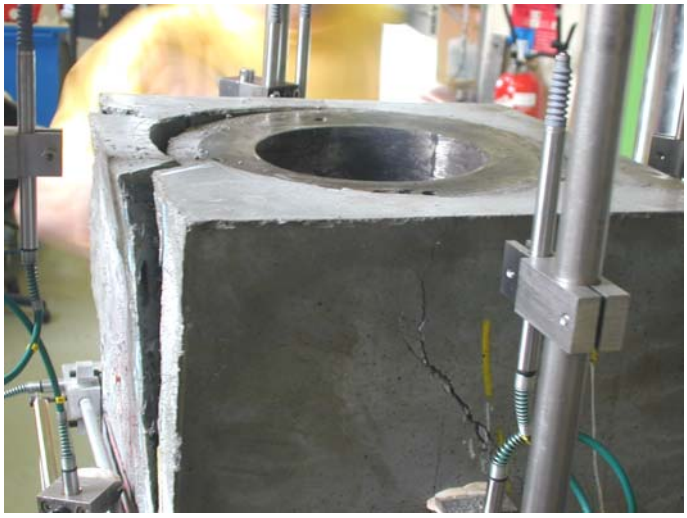

Figure 9. External instability at failure, block 7.

Non-linearity of the global curve force vs. axial displacement can be detected at 0.8 times F_{prg}, corresponding to first visible (fine) cracks. More significant non-linearity of transverse strains (Fig. 10) was observed from about 3000 kN (0.9 times F_{prg}). This lower ratio, as compared to 4T15 and 7T15 blocks made of the same material, consistently indicate that thickening of the 12T15 blocks might be desirable for ensuring a comparable pseudo-ductility and margin with respect to the maximum applicable load.

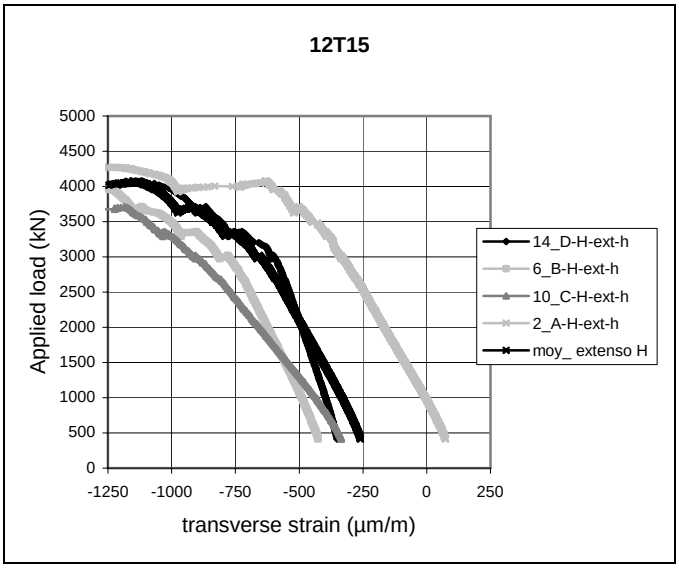

Figure 10. Block 8. Transverse strains at higher level (from top, 0.7 times the side length).

3.4 *Blocks 10 to 12 for 7T15S units*

The global behavior of the blocks is represented in terms of applied load vs. average axial global displacement, including settlement at the ends, for blocks 10 to 12 corresponding to 7T15S units with the Diwydag system (Fig. 11), after the first phase of cycles, which explains the non-zero origin of the curves. Maximum loads reached 4347, 4042 and 4111 kN respectively, which represents an average ratio of the ultimate load with respect to F_{prg} equal to 2.134. The minimum to maximum amplitude represents a variation of ± 3.6 %.

For these blocks non-linearity before the peak is significantly more pronounced, so that the maximum load is reached with corresponding vertical displacements higher than 5 mm. Occurrence of non-linearity takes place between 1550 and 1950 kN (0.8 to 1.0 times F_{prg}). Namely, first (fine) cracks have been observed at 0.8 times F_{prg} (blocks 10 and 11) and 1.0 F_{prg} (block 12). However the load goes on increasing with a still high stiffness and an important safety margin during this phase, and important transverse yielding is observed mainly at the peak (Fig. 12). Due to thick UHPFRC sides around the anchor plate, sudden bursting of the block seems to be prevented and opening of the splitting cracks is rather smoothly controlled for a displacement-controlled phase of the test. Moreover, part of the global axial settlement (about 1 mm) is due to local yielding of the steel anchor plate in correspondence to the cylinder through which load is applied (Fig. 13a, b).

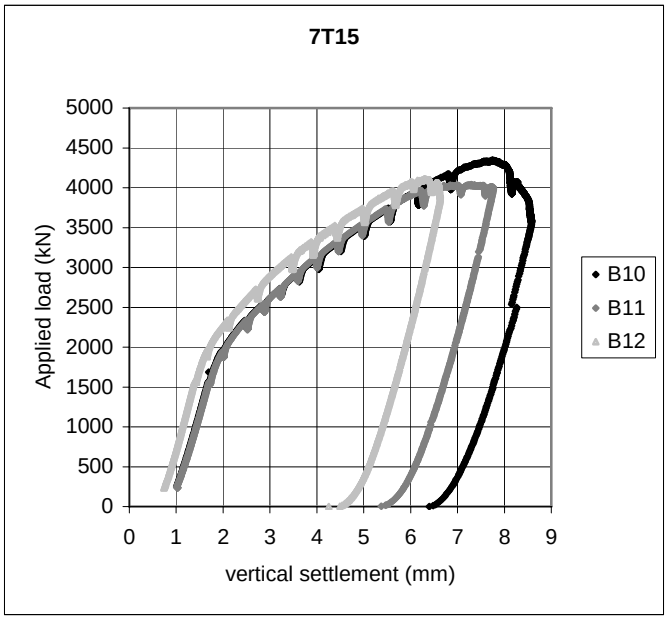

Figure 11. Load vs. axial global settlement, blocks 10 to 12.

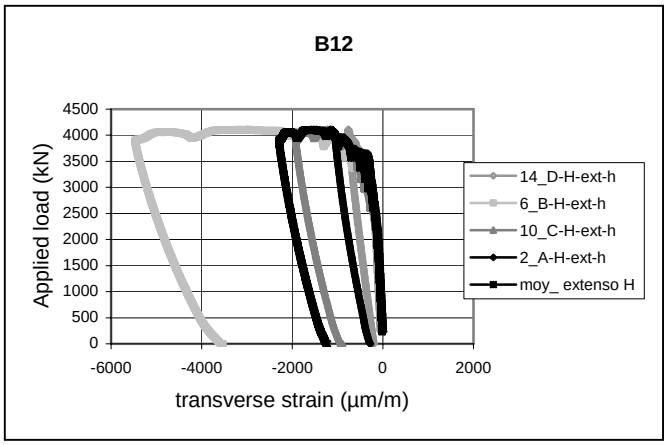

Figure 12. Block 12. Transverse strains at higher level (from top, 0.7 times the side length).

Figure 13. Punching of the steel anchor plate. a) Block 10 after failure. b) Block 11 after failure.

3.5 *Crack development – cycles and stabilization*

Besides the global behavior of the blocks and the safety margin concerning the maximum load capacity, the testing procedure of ETAG 13 requires checking the strain stabilization during load cycles from 0.12 to 0.8 times F_{prg}. The criterion is given by (1) :

$$\frac{\varepsilon_n - \varepsilon_{n-4}}{\varepsilon_4 - \varepsilon_0} \leq 0.33 \qquad (1)$$

It was not clear whether this verification should be done for each channel corresponding to horizontal or vertical strain ε. Due to the recording process, maximal strain values were determined at the maximum load of the cycle, with a 10 kN precision in terms of load and about 1 µm uncertainty for the distance measurement. In some cases, the strain evolutions from cycle 0 to 4, and possibly for cycle 10 to 14, were so low that each term of the ratio was only some 10^{-6}. It was thus agreed that for a strain evolution from cycle *n-4* to *n* corresponding to less than 10 µm, stabilization could be considered as obtained, whatever the value of the criterion. It was also considered that the 0.01 precision of the ratio could not be expected from the present measurements, therefore when the criterion was equal to 0.35 the stabilization was also deemed as satisfied. Finally, when stabilization was not obtained after 10 cycles, it was decided to apply only 4 more cycles, since the process could not be continued without further indication, and it was decided to go on with the ultimate phase of the test.

Considering the tested blocks, only blocks 4, 5, 8, 9, 11 and 12 had stabilized strains after 10 cycles. But for blocks 1 and 2 only one vertical strain record did not verify the criterion, and for blocks 6 and 10 only one horizontal strain record did not verify it. For block 3, only vertical strains of sides B and D were in excess, which was not related to clear damage. In the case of vertical strains, scatter due to sensor positioning on a rough surface might partially explain the difficulty. As a first experience gained in applying ETAG 13 procedure, it seems that in the present case this verification may have become time-consuming, not fully objective, and not clearly related to critically evolving cracks. In sum, strain stabilization as expected by ETAG 13 seems to hardly make sense for UHPFRC blocks, since possible evolution appears as hardly correlated to presence of the further critical cracks which appear on the upper part of the sides of the blocks due to induced transverse tension. As a clear result of this phase, one would be just able to conclude that for all blocks except 3, 4 and 12, first fine cracks were made visible during this cyclic loading process. Verification of the stabilization criterion hardly depends on the side considered, which may be consistent with the role of casting direction on the fiber orientation and local defects, for these rather thin parts under tension.

3.6 *Crack development to failure*

Survey of cracks was carried out during the following stage of the tests every 0.2 or 0.1 times F_{prg} depending on their observed progressive development. Crack initiation systematically took place in the middle part of one side. This side corresponded to the side up during casting for two thirds of the blocks (due sometimes to thinner UHPFRC cover of the pre-stressing duct on this side), it could also correspond to the lateral sides during casting with a possibly unfavorable fiber orientation in a straight zone for fresh concrete flow. As expected, cracks were systematically parallel to the loading direction and corresponded to indirect transverse tension within the UHPFRC ligament around the anchoring device. Their progressive extension was noticed especially when the volume of UHPFRC is relatively important (Fig. 14). Local hardening related to fiber anchoring can also have led to multiple parallel cracking (Fig. 15).

Figure 14. Progressive vertical development of splitting cracks left) Block 11 side A. right) Block 12 side C.

Figure 15. Progressive multiple cracking. Block 9 side C.

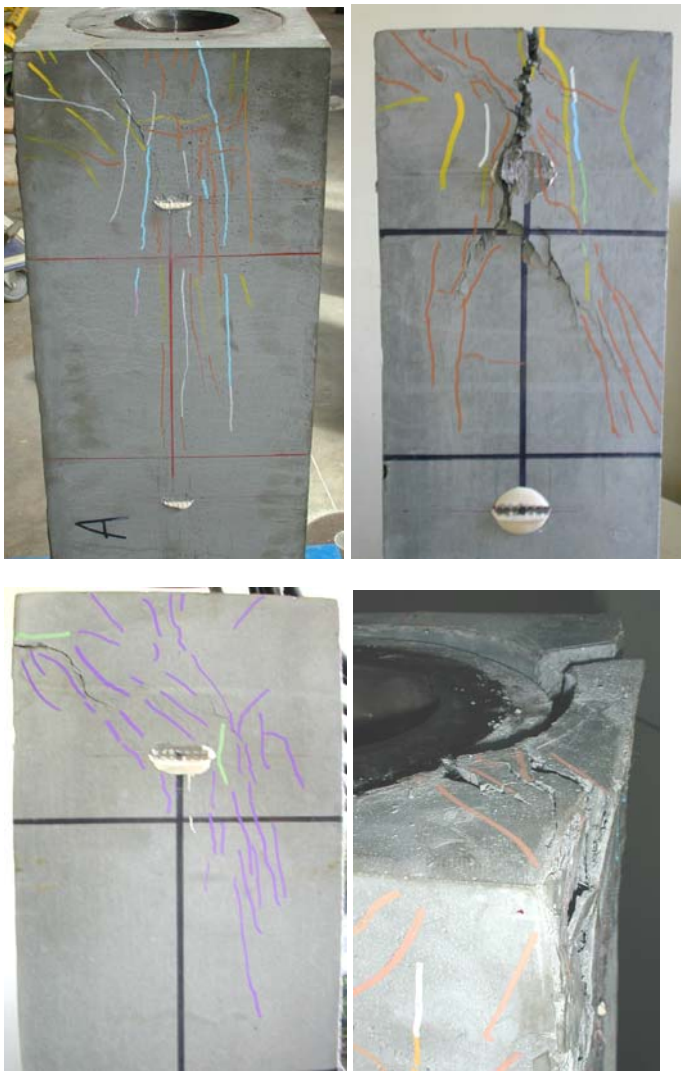

Figure 16. First vertical cracks (splitting), multiple parallel branching, and final diagonal cracks due to instable failure mechanism. Top, left) Block 8. Top, right) Block 3. Bottom, left) Block 4. Bottom, right) Block 7.

Independently of the block scale, final failure, especially in case of instability, produced different superimposed crack patterns, all of them corresponding to UHPFRC lateral or diagonal bursting (edge ejection) associated to punching of the block by the steel anchor plate (Fig. 16).

3.7 *Interpretation and sensitivity to test conditions*

Due to possible initiation of the cracks by local defects (Fig. 3, Fig. 13) no clear direct correlation was found between the load corresponding to first cracking and the size of the specimen (side, or side minus the duct thickness, or area of the UHPFRC cross-section …). However, for the same material and pre-stressing kits of similar shape, the ultimate strengths exhibit linear variations with the side of the block (Fig. 17). Yet for the blocks tested corresponding to 4T15S, 7T15S and 12T15S units, these loads are not in the same proportion as expected design loads F_{prg}. It is thus suggested that, if a similar acceptable safety margin is to be ensured, the side of the blocks

should be adapted accordingly, depending on the expected unit and corresponding F_{prg}. Further non-linear F.E. analyses calibrated on present results and accounting for the precise diffusion mechanisms around the pre-stressing anchor, would also be helpful for rationally optimizing the block geometry.

Moreover, as shown Fig. 14, the development of splitting cracks in the middle of the block sides may reach a depth twice as long as the block side. In order to get experimental results not disturbed by end effects, it is recommended that the block aspect ratio is higher than 3, even if due to the conical shape of the pre-stressing device an aspect ratio of 2 is assumed as sufficient according to ETAG 13.

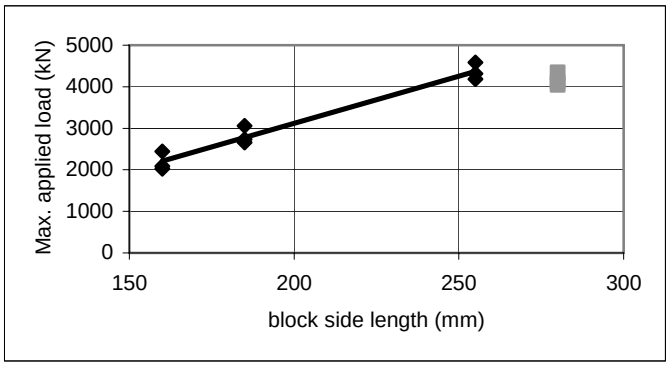

Figure 17. Block capacity as a function of its side length.

4 CONCLUSION

Experimental validation of innovative design of UHPFRC anchor blocks for post-tensioning tendons was carried out, following provisions of ETAG 13. Some possible improvements of the testing procedure have been identified.

In the tested configurations, fiber capacity within UHPFRC proved to be sufficient for dispensing of classical transverse reinforcement, by ensuring a safety margin ranging from 1.3 up to 2.1 when comparing the ultimate load with design capacity F_{prg}. Especially for the thick enough blocks, scatter of the results is remarkably low.

As expected, the failure mechanism was initiated by indirect tension perpendicularly to the applied loads, cracking was observed in the middle of lateral sides at about 0.7 times the side length from the loaded end. Visible cracks and induced non-linearity due to them were obtained from 0.8 to 1.2 times $F_{prg,}$ yet local hardening UHPFRC behavior proved to be activated for ensuring efficient confinement.

Design, dimension optimization and formal agreement of such blocks, should be pursued, taking benefit of the present results, for delaying crack onset and ensuring a more homogeneous safety margin for the different block sizes corresponding to varied pre-stressing units.

5 ACKNOWLEDGEMENT

This experimental program has been carried out within the R&D "National Project" MIKTI, funded by the Ministry for Public Works (DRAST / RGCU) and managed by IREX. It has been supervised by a committee chaired by J. Resplendino (CETE de Lyon), also chairman of the *fib* TG 8.6 mirror group. Eiffage Construction, Lafarge and VSL are mentioned for their contribution in specimens preparation. The authors are also pleased to thank A. Mellouk and F.-X. Barin from LCPC Structures Laboratory for their help in the experimental realizations. Advice of R. Chaussin from ASQPE (French Association for the Quality of Pres-stressing) for validation of the experimental program is also gratefully acknowledged.

REFERENCES

AFGC-SETRA, 2002. *Ultra High Performance Fibre-Reinforced Concretes. Interim Recommendations*. Bagneux: SETRA.

Behloul et al. 2004. Seonyu Ductal® footbridge. In *Concrete Structures: the challenge of creativity, Proc. fib Symp. Avignon, 26-28 April 2004*. Paris: AFGC.

Boulay, C. et al. 2004 Safety of VHSC structures under concentrated loading: experimental approach, *Magazine of Concrete Research* 56(9):523-535.

Bouteille S. & Resplendino J. 2005. Derniers développements dans l'utilisation des bétons fibrés ultra-performants en France. In *Performance, Durabilité, esthétique, Proc. GC'2005, Paris, 5-6 October 2005*. Paris: AFGC.

EN 1992-2: 2005. Eurocode 2 – Calcul des structures en béton – Partie 2 : Ponts en béton – calcul et dispositions constructives, *CEN*.

EOTA, 2002. Guide d'agrément technique européen sur les kits de mise en tension de structures précontraintes (GATE 013). Bruxelles: EOTA.

Ganz H. R. & Adeline R. 1997. Mini-anchorages for Reactive Powder Concrete. In *f.i.p. Int. Conf. On new technologies in structural engineering, Lisbon, july 1997*.

Hajar Z. et al. 2004. Construction of an ultra-high performance fibre reinforced concrete thin-shell structure over the Millau Viaduct toll gate. In *Concrete Structures: the challenge of creativity, Proc. fib Symp. Avignon, 26-28 April 2004*. Paris: AFGC.

Toutlemonde, F. et al. 2005 Innovative design of ultra-high performance fiber-reinforced concrete ribbed slab : experimental validation and preliminary detailed analyses. In Henry Russel (ed.), *Proc. 7th Int. Symp. On Utilization of High Strength / High Performance Concrete, Washington D.C. (USA), 20-22 June 2005*. ACI-SP 228, 1187-1206.